Journal Name

ARTICLE TYPE

Cite this: DOI: 10.1039/xxxxxxxxxx

Determination of the exciton binding energy and effective masses for methylammonium and formamidinium lead tri-halide perovskite semiconductors

Krzysztof Galkowski,*[a,b] Anatolie Mitioglu,[a] Atsuhiko Miyata,[a] Paulina Plochocka,[a] Oliver Portugall,[a] Giles E. Eperon,[c] Jacob Tse-Wei Wang,[c] Thomas Stergiopoulos,[c] Samuel D. Stranks,[c] Henry J. Snaith,[c] and Robin J. Nicholas[c]

Received Date
Accepted Date

DOI: 10.1039/xxxxxxxxxx

www.rsc.org/journalname

The family of organic-inorganic halide perovskite materials has generated tremendous interest in the field of photovoltaics due to their high power conversion efficiencies. There has been intensive development of cells based on the archetypal methylammonium (MA) and recently introduced formamidinium (FA) materials, however, there is still considerable controversy over their fundamental electronic properties. Two of the most important parameters are the binding energy of the exciton (R^*) and its reduced effective mass μ. Here we present extensive magneto optical studies of Cl assisted grown $MAPbI_3$ as well as $MAPbBr_3$ and the FA based materials $FAPbI_3$ and $FAPbBr_3$. We fit the excitonic states as a hydrogenic atom in magnetic field and the Landau levels for free carriers to give R^* and μ. The values of the exciton binding energy are in the range 14 - 25 meV in the low temperature phase and fall considerably at higher temperatures for the tri-iodides, consistent with free carrier behaviour in all devices made from these materials. Both R^* and μ increase approximately proportionally to the band gap, and the mass values, 0.09-0.117 m_0, are consistent with a simple **k.p** perturbation approach to the band structure which can be generalized to predict values for the effective mass and binding energy for other members of this perovskite family of materials.

1 Broader context

The recent development of organic/inorganic perovskite semiconductors has had a dramatic impact on the field of thin-film solar cells leading to efficiencies of over 20% in materials such as $MAPbI_3$. We have recently shown that significant factors contributing to their remarkable performance are the small excitonic reduced effective mass and the small exciton binding energy. Expanding the perovskite family to materials with a range of different band gaps is opening up the potential of this materials system for a range of different applications, including the design of tandem PV cells and other optoelectronic components such as lasers and light emitting diodes. Knowledge of basic materials parameters such as the effective masses of the charge carriers is vital to the use and design of devices using perovskites. Here we show that the effective masses remain small in this system up to band gaps as high as 2.3 eV, as found in $MAPbBr_3$ and the exciton binding energy in this system is also much smaller than previously reported. This suggests that sophisticated devices using large band gap perovskites can be expected to show free carrier behaviour at room temperature and will make device design significantly easier. Exchanging the organic cations (Methyammonium or Formamodimium) is also shown to have very little effect on their bandstructure, suggesting that they can be used interchangeably to enhance device performance and stability.

2 Introduction

Organic-inorganic hybrid materials, in particular the tri-halide perovskites, have been driving a rapid series of breakthroughs in the field of photovoltaic (PV) devices with conversion efficiencies already up to 20%[1] and beyond in devices which can be produced on cheap non-crystalline substrates by both vapour deposition[2] and solution processing[3,4].Their excellent performance originates from the combination of strong absorption[5] and long diffusion lengths[6,7]. In addition, the ability to generate a family of materials with band gaps which can be tuned by alloying the halide elements[8] and modifying the organic ions[9], allows the band structure to be optimized and offers the possibil-

[a] Laboratoire National des Champs Magnetiques Intenses, CNRS-UJF-UPS-INSA, 143 Avenue de Rangueil, 31400 Toulouse, France
[b] Institute of Experimental Physics, Faculty of Physics, University of Warsaw - Pasteura 5, 02-093 Warsaw, Poland
[c] University of Oxford, Clarendon Laboratory, Parks Road, Oxford, OX1 3PU, United Kingdom; E-mail: r.nicholas@physics.ox.ac.uk

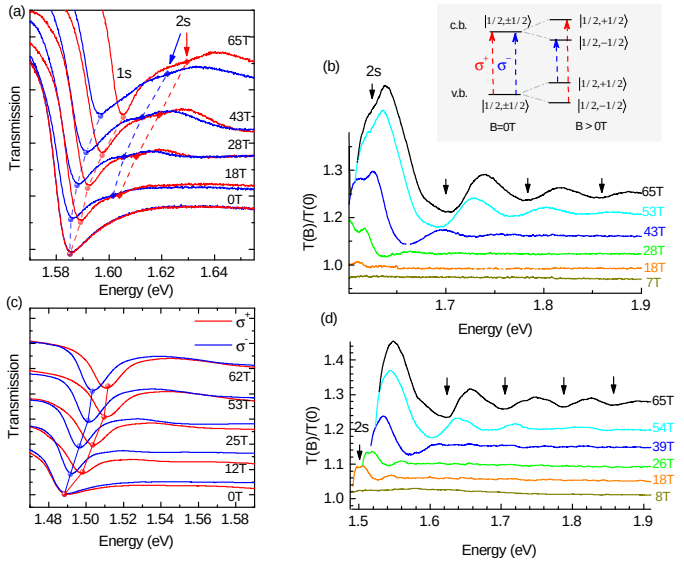

Fig. 1 (a)-(b) and (c),(d) typical low temperature transmission data taken using a long pulse technique for $MAPbI_{3-x}Cl_x$ and $FAPbI_3$ respectively. Red and blue lines in panels (a) and (c) correspond to two σ^+ and σ^- polarized light respectively. The selection rules for both polarizations are shown in the inset. Different colors on panels (b) and (d) correspond to the data taken at different values of magnetic field.

ity of their use in multi-junction cells with even higher efficiencies. In addition to PV devices the perovskite family of semiconductors has also been used to successfully demonstrate light emitting diodes[10], lasers[11,12] and photodetectors[13]. The chemical structure of these perovskite semiconductors is ABX_3 where A=$CH_3NH_3^+$ = MA (MethylAmmonium) or A=$CH(NH_2)_2$ = FA (FormAmidinium), B=Pb^{2+}; and X = Cl^-, I^- or Br^-, or an alloyed combination of these), where the majority of effort has gone into the development of the MA family[14–16]. Although there have been tremendous strides made in developing working PV devices using these perovskites[2–4,9,17–21] there have been far fewer studies reported on their fundamental electronic properties. Basic physical parameters such as the carrier effective masses (μ) or the exciton binding energy (R^*), remain poorly characterized and their values are still controversial. Knowledge of these parameters is crucial for optimization and control of solar cells based on the organic-inorganic tri-halide perovskite family.

From the point of view of applications the binding energy of the exciton is critical for determining the operation of devices. This value compared with the thermal energy (kT $\simeq$ 25 meV at 300K) determines whether the photo created carriers will dissociate or will need to be separated by an additional junction in a PV device. Until very recently the reported values of binding energy were highly controversial and covered a wide range: For $MAPbI_3$ values from 2 to 55 meV[5,22–27] have been reported with values at the lower end of the range now becoming more common in the literature[25–27]; and for $MAPbBr_3$ it has been suggested that R^* could be as high as 70 meV[5]. Recently, we[28] have shown that by using magneto optical studies an exact determination of the binding energy of the exciton and effective mass of the carriers for $MAPbI_3$ is possible at low temperatures from the measurement of sequences of higher states for the excitonic transitions and the quantization of the free carrier states into Landau levels. We now extend this type of study to the wider family of organic-inorganic perovskite tri-halides to establish their basic materials parameters and enable their use in the design of the new generation of opto-electronic components based on these materials. In particular we report studies of the FA-based analogues, which appear to be more thermally stable than their MA counterparts[9,13] and which have been mixed with MA to give the highest device performance to date[29].

Here, we present low temperature studies of magneto optical absorption spectroscopy, which directly probes basic electronic parameters such as the binding energy of the neutral free exciton and the excitonic reduced effective mass (μ) of the carriers for the different families of hybrid inorganic-organic perovskite materials. We have investigated the methylammonium and formamidinium lead halide family with band gaps in the range 1500 - 2233 meV. The value of both the exciton binding energy and the reduced effective mass increase approximately proportionally to the band gap and their values are consistent with a simple two band **k.p** perturbation theory approach to the band structure which can be generalized to predict values for the effective mass and binding energy for other members of this perovskite family of materials.

3 Results and discussion

Typical low temperature magneto transmission spectra measured at 2K for thin films (≈350nm thick) deposited onto glass are shown for representatives of the two perovskite families in Fig 1 at a series of magnetic fields. The panels (a)-(b) show the results for $MAPbI_{3-x}Cl_x$ and (c) - (d) results for $FAPbI_3$. The spectra shown in Fig 1(a) and (c) exhibit one very strong minimum, which corresponds to the strongest absorption originating from the 1s state of the neutral free exciton. Data taken for different circular polarizations (red and blue lines) clearly show Zeeman splitting, according to the selection rules for circularly polarized absorption presented in the inset in Fig 1(b)[5,25,30,31], which shows the spin split electron and hole states of the conduction and valence band. Also visible in Fig 1(a) is the 2s state which appears as a further weak absorption. To observe absorption from higher electronic states the measurements have been extended to much higher energies. As the absorption to the higher states is weaker we plot the data as differentials; the spectrum in high magnetic field is divided by the spectrum at zero magnetic field (Fig 1(b),(d)) to show the additional field induced absorptions. Here we show only one circular polarization, as the spin splitting is not resolved on such a large energy scale. In the differential spectra we observe the 2s state more clearly (Fig 1(b),(d)) and a sequence of additional minima marked by arrows. The absorption minima become more pronounced with the increase of the magnetic field and their energy blue shifts.

To follow the absorption minima to higher energies, we extended the measurements to higher magnetic field (B>70T) using a short pulse technique where we measure the transmission of a monochromatic (laser) source through the sample as a func-

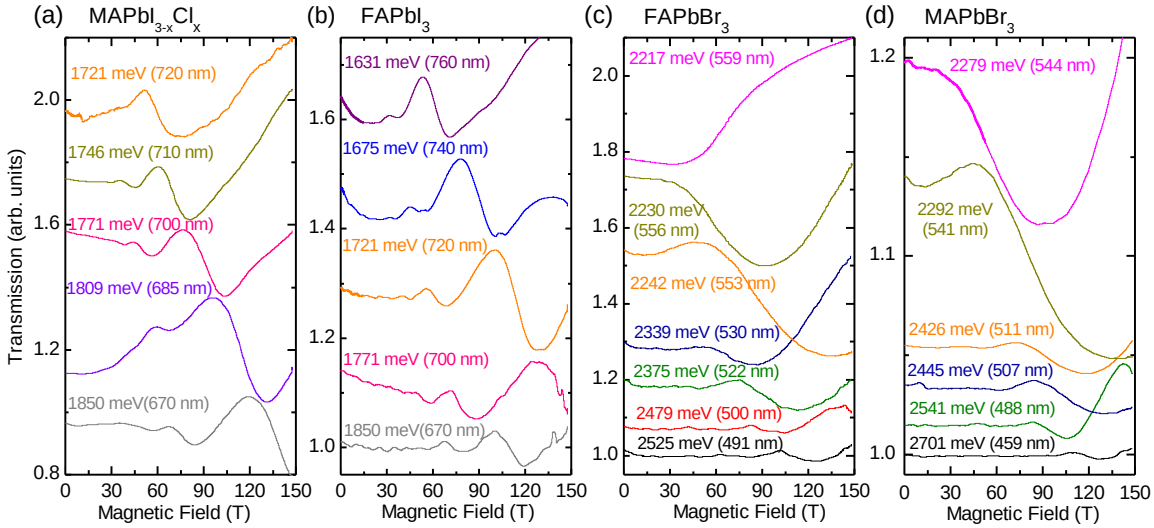

Fig. 2 (a) - (d) typical results of the low temperature monochromatic transmission as a function of magnetic field obtained by using the short pulse technique for $MAPbI_{3-x}Cl_x$, $FAPbI_3$, $FAPbBr_3$ and $MAPbBr_3$ respectively. The transmission signals are normalized to 1 at zero magnetic field and offset to improve visibility. Different colors mark different laser energies.

tion of magnetic field. Typical results obtained for three different samples are presented in Fig 2. In all the spectra we observe well developed minima as a function of magnetic field. This technique gives the equivalent of a horizontal slice of the absorption spectrum as a function of magnetic field and has transmission minima at magnetic fields corresponding to resonant transitions between the free carrier Landau levels of the conduction and valence band and also for the creation of excitonic states as shown schematically in Fig 3. It is very powerful for high magnetic fields and high energies where the transition energies are a strong function of magnetic field and the level broadening is larger. This is particularly important for compounds such as $FAPbBr_3$, where the band gap is at a rather high energy (around 2232 meV) and the effective mass is larger, making the results from the short pulse measurements critical to determine the correct value for the effective mass of the free exciton.

In order to extract the binding energy of the free exciton and the effective mass of the carriers we have analyzed the position of the absorption energy as a function of magnetic field. The results of this analysis are presented as fan diagrams in Fig 4. The circles and stars correspond to the minima observed in the long pulse spectra and the fast pulse magneto-transmission respectively. To fit the data we have used the same theoretical approach as previously used[28] for $MAPbI_3$: (i) the absorption close to the energy gap is assumed to originate from hydrogen like behavior typical for free excitons and this behaviour is stronger in the tribromide samples where the exciton binding energy is found to be larger, (ii) the higher energy part of the spectrum reflects the free carrier behavior: interband transitions between Landau levels in the valence and conduction bands[32]. The hydrogen-like behavior can be modelled using the numerical solutions of the hydrogen atom in a strong magnetic field calculated by Makado and McGill[33]. The energy of the free exciton transitions $E_{n,0}(\gamma)$ can be described using only the dimensionless parameter $\gamma = \hbar\omega_c/2R^*$,

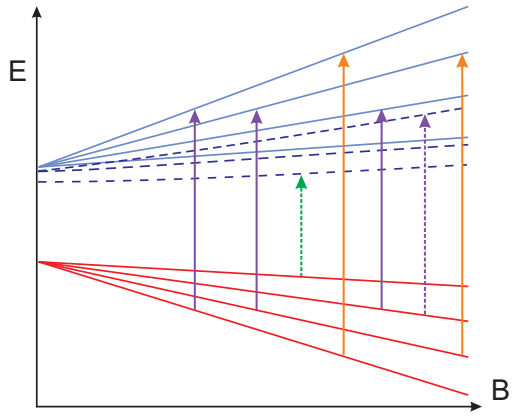

Fig. 3 A schematic view of the Landau levels (solid lines) and excitonic states created by excitation from the valence band (dashed lines) as a function of magnetic field. A sequence of transitions which might be observed for 3 different laser energies are shown as different colours. The solid arrows represent free carrier transitions and the dashed arrows show excitonic transitions.

where $\hbar\omega_c = \hbar eB/\mu$ is a cyclotron energy directly proportional to the magnetic field and inversely proportional to the reduced exciton effective mass μ defined by $1/\mu = 1/m_h + 1/m_e$, where $m_{h,e}$ are the effective masses of the hole and electron respectively. For high magnetic fields where $\gamma > 1$ the free carrier inter Landau level transitions become dominant with transition energies given by

$$E(B) = E_g + (n + \frac{1}{2})\hbar\omega_c \pm \frac{1}{2} g_{eff}\mu_B B \quad (1)$$

where E_g is the energy band gap, n = 0,1,2... is a Landau Level quantum number which is conserved in the transition between hole and electron levels, g_{eff} is an effective g factor for the Zeeman splitting and μ_B is the Bohr magneton. As the Zeeman effect only introduces a constant splitting in the absorbtion spectra it can be introduced in a similar way into the hydrogen like model for the excitons. It is important to note that the Zeeman splitting was not observed in our previous studies[28] as circular polarized light was not used.

The results of the fitting for each sample are shown in Fig 4 by solid and dashed lines for the excitonic states in the two polarizations. Transitions between Landau levels are marked by grey lines. In the case of interband transitions the only fitting parameter is the reduced mass of the exciton. As there is only one fitting parameter the high magnetic field and high energy data give a strong constraint on the exciton reduced mass. By keeping the same effective mass we can then fit the hydrogen - like transitions using the exciton binding energy (R^*) as another fitting parameter. Moreover, observation of both the 1s state and in particular the 2s state, which is only observable once its oscillator strength has been enhanced by the magnetic field, is very important. Both of these levels originate from the same Landau level giving a very strong constraint in the determination of the exciton binding energy, which scales for a 3D hydrogen atom in zero magnetic field as:

$$E_n = E_g - \frac{R^*}{n^2} \quad (2)$$

where E_n is the energy of n-th excitonic level and $R^* = R_0\mu/m_0\varepsilon_r^2$, where R_0 is the atomic Rydberg constant, m_0 is the free electron mass and ε_r is the relative dielectric constant. Results of the analysis for different compounds are summarized in table 1.

The exciton effective masses are in good agreement with recent predictions (μ=0.09 -0.1 m_0) of density functional theory for the tri-iodides where the theory has been adjusted to fit the experimental values of the band gap[24,34]. Fig 5 and Table 1 show that at 2K both μ and R^* are weakly increasing functions of the material band gap. The relatively simple band structure of these materials, which have non-degenerate band edges which are relatively isotropic and have similar effective masses suggests that they can be described by a simple semi-empirical two band **k.p** Hamiltonian approach[35] with effective masses for the electron and hole given by

$$\frac{1}{m_{e,h}} = \frac{1}{m_0}|(1 \pm \frac{2m_0|P|^2}{E_g})| \quad (3)$$

2K, Orthorhombic phase

Compound	E_g (meV)	R^* (meV)	μ (m_e)	ε_{eff}	g_{eff}
$FAPbI_3$	1501	14	0.09	9.35	2.3
$MAPbI_{3-x}Cl_x$	1596	14	0.10	9.85	2.3
$MAPbI_3$	1652	16	0.104	9.4	
$FAPbBr_3$	2233	22	0.115	8.42	
$MAPbBr_3^*$	2292	25	0.117	7.5	

High Temperature Tetragonal phase

Compound	E_g (meV)	R^* (meV)	μ (m_e)	ε_{eff}	*Temperature* (K)
$FAPbI_3$	1521	10	0.095	11.4	140-160
$MAPbI_{3-x}Cl_x$	1600	10	0.105	11.9	190-200
$MAPbI_3$	1608	12	0.104	10.9	155-190
$FAPbBr_3$	2294	24	0.13	8.6	160-170

Table 1 The parameters of the fit full Landau fan chart for four different compounds in the low temperature, orthorhombic and the higher temperature, tetragonal phases. *The data for the $MAPbBr_3$ do not show a detectable 2s state and therefore have a significant errors of $\pm$10% for μ and $\pm$20% for R^*.

where the Kane energy is $2m_0(|P|^2)$, with $P = < \psi_{VB}|i\hbar\frac{\partial}{\partial x}|\psi_{CB} >$ which is the momentum matrix element coupling electron wavefunctions in the conduction and valance bands, which is taken to be isotropic. The valence band consists mostly of Iodine p-like states and the conduction band is a mixture of hybridized Lead s and p-like states[1,34,36] in a similar form to III-V semiconductors. The value of the excitonic reduced mass is therefore

$$\frac{1}{\mu} = |\frac{1}{m_e}| + |\frac{1}{m_h}| = \frac{4m_0|P|^2}{E_g} \quad (4)$$

Direct calculations of the Kane energy predict it to be in the range 5.3 - 6.3 eV for these materials[25,37] although recently calculated theoretical masses suggest a higher value[24,34]. Fig 5 shows that the reduced mass is quite well described using the band gap obtained from Eq. 4 and a somewhat larger value of 8.3 eV for the Kane energy which fits all members of the family studied to within 10%. There is no significant difference between the material made using different organic cations (MA or FA) other than that associated with the small changes in band gap probably associated with changes in lattice parameter.

The effective Rydberg is somewhat more material dependent, varying from 14 - 25 meV approximately as:

$$R^* = 0.010 * E_g \quad (5)$$

with values approximately 3 times smaller than previously reported from magneto-optical studies where only the 1s state was observed[5], but in good agreement with the value of 15 meV deduced by Even et al[25] by fitting a much more highly resolved zero field exciton absorption spectrum. We attribute this difference to the much poorer resolution of the excitonic transitions in the previous magneto-optical studies and to the analysis of only a single excitonic transition. The low temperature values deduced here

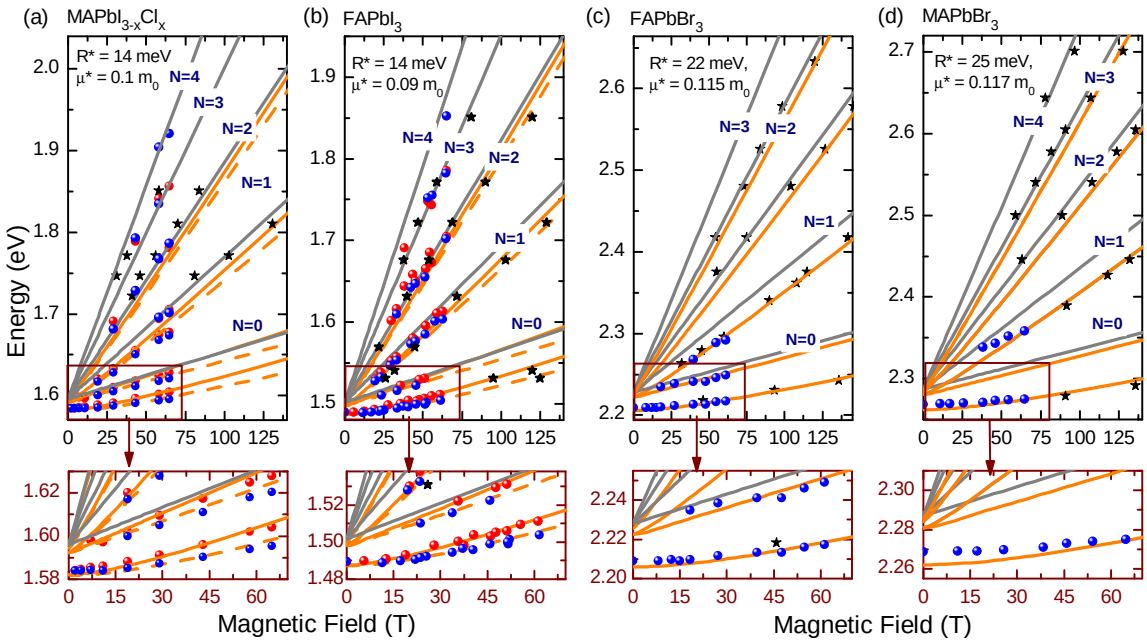

Fig. 4 (a)-(d) transition energies obtained from the experimental data and results of the fit to the data for $MAPbI_{3-x}Cl_x$, $FAPbI_3$, $FAPbBr_3$ and $MAPbBr_3$ respectively. The red and blue points correspond to the polarization resolved minima in the absorption for σ^+ and σ^- respectively. The stars are the data obtained during the short pulsed measurements, where polarization was not used. The long pulsed data are also not polarization resolved for the $FAPbBr_3$ and $MAPbBr_3$ samples. The results of the theoretical fit are shown by grey and orange lines. Grey lines correspond to the interband transitions between Landau levels in the valence and conduction bands. The orange lines show the strongly bound levels of the hydrogen - like exciton. In (a) and (b) the Zeeman split transitions are shown by the solid and dashed lines. Below each graph the low field and low energy part of the full fan chart diagram is enlarged.

are all less than or comparable to the thermal energy at room temperature and suggest therefore that the entire family of organic-inorganic tri-halide perovskites can be expected to show rapid excitonic ionization at 300K. This conclusion is strengthened by the temperature dependent reduction of the exciton binding energy discussed below.

We can use the conventional formula for the effective Rydberg to define an effective dielectric constant ε_{eff} which takes account of the screening of the Coulomb potential by the lattice. This value, in the range 7.5-9.8, is intermediate between the low (ε_0 = 25.7)[38] and high (ε_∞ = 5.6) frequency values[34,39] and decreases slightly with the increasing values of μ and R^* probably due to the reduction in size of the exciton Bohr radius and differences in the crystal structure. This behaviour is characteristic of highly polar materials with strong electron-phonon coupling. This was first discussed by Pollman and Buttner[40] and by Kane[41] who showed that in II-VI and I-VII materials ε_{eff} was intermediate between the two values ε_0 and ε_∞. In TlCl for example, a material with comparable parameters (ε_∞ = 5.4, ε_0 = 37.6, μ=0.18m_0) it was found that ε_{eff}=2.48ε_∞. In perovskites where there are multiple polar phonon modes, including rotational motion of the MA cations[25,34,38,39] such a calculation is more difficult but has recently been reported[42] giving results consistent with the proposal that the value of ε_{eff} will again be intermediate between ε_0 and ε_∞. It is noticeable that the values for ε_{eff} are significantly lower for the tri-bromides, where the higher reduced masses cause the binding energy to be larger, with a consequent reduction in the

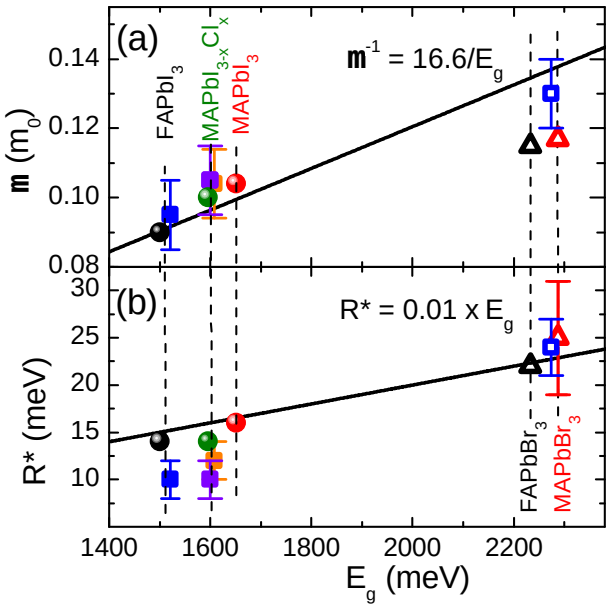

Fig. 5 (a), (b) Effective mass and binding energy as a function of the energy gap respectively. Black (red) symbols mark results for FA (MA) iodides (full symbols) and bromides (open symbols) at 2K. Green circles show results for the mixed halide $MAPbI_{3-x}Cl_x$ at 2K. Squares show values for the FA (blue), MA (orange) and mixed halide (purple) materials deduced for the higher temperature tetragonal phase measured in the temperature ranges given in Table 1. The black solid lines show a linear fit to the data.

strength of the screening. Given the higher uncertainty in the values of R* for the $MAPbBr_3$, however, we do not consider the difference in ε_{eff} between the MA and FA tri-bromides to be significant at present.

The values for g_{eff} are slightly larger than reported previously[5] and are consistent with a linear spin splitting and show no evidence for the predicted Rashba splitting which it has been suggested may occur for some crystal structures in the high temperature phase[31,35].

In order to be useful for understanding the properties of devices operating at room temperature it is important to expand the magneto-optical studies to as high a temperature as possible, in particular as all the family of organic-inorganic tri-halide perovskites show a series of phase transitions at higher temperatures to more symmetric structures. The tri-iodides transform from an orthorhombic to a tetragonal structure with increasing temperature at around 150K accompanied by a small decrease in band gap. The tri-bromides are cubic at room temperature[8,9], and transform to tetragonal in the alloy family $FAPbBr_{3-x}I_x$ at around x=0.6, although when plotted as a function of the pseudocubic lattice parameter a^* the band gap is a continuous function across the phase transition[9]. As a function of temperature the tri-bromides transform to a tetragonal structure at around 240K and then become orthorhombic below 150K[43]. The transition from the cubic to the tetragonal structure appears to have no significant influence on the band gap as measured either by absorption (SI Fig 3) or reflectivity[44], but the transition to a tetragonal structure at low temperatures produces a small shift in band gap of around 10 meV.

We have repeated the magneto-optical study at higher temperatures (140-200K), sufficiently high to be in the higher temperature crystallographic phase for each material as determined from the absorption measurements (SI Fig. 3). The absorption spectra are shown in the supplementary information (SI Fig. 1, Fig. 2) and the fan diagrams in Fig6. These are again fitted to give the band parameters for the high temperature phase shown in Fig 5 and Table 1. The experimental values deduced for the high temperature results have significantly greater statistical and systematic errors as fewer transitions are seen and these are less well resolved. In particular the non-observation of a 2s state in the intermediate field range of 10 - 65 T, where it was strongest at low temperatures, makes the measurement of the exciton binding energy significantly less certain. An additional factor also is that it has been shown that[45] the phonon contribution to the dielectric screening is reduced by the magnetic field due to the increasing exciton binding energy and so the values of R* deduced from the resonances observed at over 50T will be an overestimate of the zero field value as discussed previously by Miyata et al[28].

In the the $MAPbI_3$ it was found[28] that the effective mass in the higher temperature tetragonal phase was essentially the same as for the low temperature phase at a similar band gap. Our results here suggest that although the values in the high temperature phase may be a few % larger than at 2K this is at the limit of the accuracy of the high temperature fits and that essentially the effective masses of the whole family of organic-inorganic tri-halide perovskites can be reasonably described in terms of the single parameter of the band gap through Eq. 4 irrespective of the crystal phase or temperature.

The phase transition to a tetragonal phase in the region of 150K is likely to be more significant for the dielectric constant and consequently the exciton binding energy, as additional collective rotational motion of the organic cations becomes allowed. This has been shown to cause an increase in the dielectric constant[46], which led Even et al[25] to propose that this could cause a decrease in binding energy to values of the order of 5 meV[25] which they again deduced from fitting the excitonic absorption. Using a similar type of analysis Yamada et al[26] have suggested that there is a continuous decrease in binding energy from 30 meV at low temperature to 6 meV at 300K, while Soufliani et al[47] report a reduction from 25 to 12 meV. The existence of a decreased exciton binding energy in the high temperature phase was supported by our previous high temperature magneto-optical measurements[28]. For all the tri-iodide materials analysed here the resonant transitions are only observed at very high fields (above 50T) but even so the exciton binding energies are reduced to values of order 10±3 meV with a corresponding increase in ε_{eff}. In addition the anomalously low diamagnetic shift of the 1s exciton state suggests that there is a field dependent increase in the 1s binding energy[45] which leads us to conclude that the low field exciton binding energy has fallen to values of order 5 meV or less. By contrast the $FAPbBr_3$ shows no significant reduction in the exciton binding energy in the higher temperature cubic state, probably because the original binding energy corresponds to a frequency which is too large to respond to the additional screening and consequently the low field diamagnetic shift is close to the theoretical prediction.

4 Conclusions

In conclusion our results provide a general relation for the low temperature exciton binding energy (5) and reduced effective mass (4), which are determined principally by the material band gap E_g for the whole organic-inorganic lead tri-halide perovskite family. The exact nature of the organic cations (MA or FA) is shown to have relatively little influence, producing only small changes in effective mass which are correlated with the changes in band gap. This suggests that simple two band **k.p** perturbation theory should enable accurate modelling of the properties of devices made from materials in this system. Our results also demonstrate that the low temperature values of the exciton binding energies are small compared to the thermal energy at 300K which makes a significant contribution to understanding the excellent performance of these devices. For the tri-iodides these values fall still further in the high temperature phase of the materials probably due to increased screening but this is not observed in the FA tri-bromides.

5 Experimental Method

Perovskite precursor synthesis: Formamidinium iodide (FAI) and formamidinium bromide (FABr) were synthesised by dissolving formamidinium acetate powder in a 1.5x molar excess of 57% w/w hydroiodic acid (for FAI) or 48% w/w hydrobromic acid (for FABr). After addition of acid the solution was left stirring for 10 minutes at 50^0 C. Upon drying at 100^oC, a yellow-white pow-

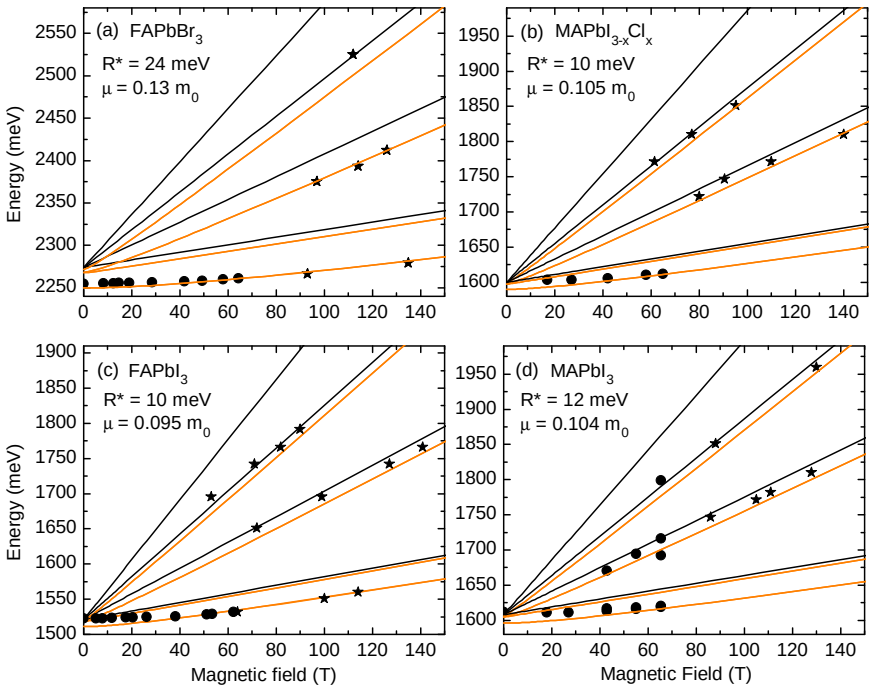

Fig. 6 (a)-(c) transition energies obtained from the experimental data and results of the fit to the data for the high temperature phases of $MAPbI_{3-x}Cl_x$, $FAPbI_3$, and $FAPbBr_3$ respectively. The circles are data obtained using long pulsed fields and the stars are data obtained during the short pulsed field measurements both using unpolarized light. Polarization was not used. The data from Miyata et al.[28] for the high temperature phase of $MAPbI_3$ are shown (d) for comparison. The results of the theoretical fit are shown by grey and orange lines. Grey lines correspond to interband transitions between Landau levels in the valence and conduction bands. The orange lines show the strongly bound levels of the hydrogen - like exciton.

der is formed. This was then washed twice with diethyl ether and recrystallized with ethanol, to form white needle-like crystals. Before use, it was dried overnight in a vacuum oven. To form $FAPbI_3$ and $FAPbBr_3$ precursor solutions, FAI and PbI_2 or FABr and $PbBr_2$ were dissolved in anhydrous N,N-dimethylformamide (DMF) in a 1:1 molar ratio, at 0.55M of each reagent, to give a 0.55M perovskite precursor solution. To form $CH_3NH_3PbI_{3-x}Cl_x$ precursor solutions, Methylammonium iodide (MAI) and lead chloride ($PbCl_2$) were dissolved in a 40% w/w DMF solution in a 3:1 molar ratio. For $MAPbI_3$, precursor solutions were prepared separately by dissolving lead iodide (PbI_2) in DMF (450 mg/ml), and MAI in isopropanol (50 mg/ml), respectively.

Film formation: All the samples were prepared in a nitrogen-filled glovebox on glass substrates cleaned sequentially in hallmanex, acetone, isopropanol and O_2 plasma. Immediately prior to the Formamidinium (FA) sample film formation, small amounts of acid were added to the precursor solutions to enhance the solubility of the precursors and allow smooth and uniform film formation. 38μl of hydroiodic acid (57% w/w) was added to 1ml of the 0.55M $FAPbI_3$ precursor solution, and 32μl of hydrobromic acid (48% w/w) was added to 1ml of the 0.55M $FAPbBr_3$ precursor solution. FA Films were then spin-coated from the precursor plus acid solution on warm (85^{o}C) substrates for 45s at 2000rpm, followed by annealing at 170^{o}C in air for 10 minutes. This gave very uniform pinhole-free layers, 350nm thick, of $FAPbI_3$ or $FAPbBr_3$.

The Methylammonium (MA) samples were prepared following methods described previously[3,48]. In brief, $CH_3NH_3PbI_{3-x}Cl_x$ films were prepared by spin-coating for 60s at 2000 rpm on warm (85^{o}C) substrates, followed by annealing at 100^{o}C in air for 1 hour. The $CH_3NH_3PbI_3$ films were prepared from a PbI_2 layer which was first deposited on cleaned glass by spin-coating at 6000rpm for 30s from a precursor solution, followed by drying at 70^{o}C for 5 min. Then the MAI layer was deposited on the dried PbI2 layer by spin-coating at 6000rpm for 30s from a precursor solution, followed by annealing at 100^{o}C for 1 hour. For the $MAPbBr_3$ films lead(II) acetate trihydrate (Sigma) and MABr (Dyesol) were dissolved in anhydrous N,N-Dimethylformamide (DMF) at a 3:1 molar ratio with a final perovskite precursor concentration of 40 wt%. Then, the solution was spin-coated at 2000 rpm (for 45 s) in a nitrogen-filled glovebox. After spin-coating, films were left to dry at room temperature in the glovebox for 5-10 minutes and then annealed at 100^{o}C for 15 minutes. The perovskite films were all sealed by spin-coating a layer of the insulating polymer poly(methyl methacrylate) (PMMA) at 1000rpm for = 60s (precursor solution 10mg/ml in cholorobenzene) on top in order to ensure air-and moisture-insensitivity.

The magneto-transmission measurements were performed in pulsed magnetic fields ≤ 70 T ($\simeq 500$ ms) in LNCMI Toulouse. A tungsten halogen lamp provides a broad spectrum in the visible and near infra-red range and the absorption was measured in the Faraday configuration with the c-axis of the sample parallel to magnetic field. The circular polarization was introduced in-situ. Rotation between σ^+ and σ^- polarized light was done by change of the direction of the magnetic field. A nitrogen cooled CCD de-

tector analyzed the transmitted light dispersed by a spectrometer. Differential transmission spectra were produced by normalizing all the acquired spectra by the zero field transmission or by signal of the halogen lamp. The sample was immersed in a liquid helium cryostat. The measurements have been performed either in superfluid or in gaseous helium. No evidence was found for sample degradation during thermal cycling. Measurements to higher fields ≤ 150 T were performed using a semi-destructive technique and pulse lengths of $\simeq 10$ μs, where transmission of a series of laser diodes and a Ti-Sapphire tunable laser through the sample was measured by fast (100MHZ) silicon detector and high speed digital oscilloscope[28,49]. The sample was mounted inside a non conducting helium flow cryostat and was cooled separately for each measurement. The magnetic fields were generated by a semi-destructive single turn coil system using 10mm coils[49,50]

6 Acknowledgements

This work was partially supported by ANR JCJC project milliPICS, the Region Midi-Pyrénées under contract MESR 13053031. We also acknowledge support by EuroMagNET II under the EU Contract Number 228043. The authors also thank: Meso-superstructured Hybrid Solar Cells -MESO NMP-2013-SMALL7-604032 project, the Engineering and Physical Sciences Research Council (EPSRC), the European Research Council (ERC-StG 2011 HYPER Project no. 279881).

References

1 H. Zhou, Q. Chen, G. Li, S. Luo, T.-B. Song, H.-S. Duan, Z. Hong, J. You, Y. Liu and Y. Yang, *Science*, 2014, **345**, 542–546.

2 M. Liu, M. B. Johnston and H. J. Snaith, *Nature*, 2013, **501**, 395.

3 M. M. Lee, J. Teuscher, T. Miyasaka, T. N. Murakami and H. J. Snaith, *Science*, 2012, **338**, 643–647.

4 J. Burschka, N. Pellet, S.-J. Moon, R. Humphry-Baker, P. Gao, M. K. Nazeeruddin and M. Graetzel, *Nature*, 2013, **499**, 316.

5 K. Tanaka, T. Takahashi, T. Ban, T. Kondo, K. Uchida and N. Miura, *Solid State Communications*, 2003, **127**, 619 – 623.

6 G. Xing, N. Mathews, S. Sun, S. S. Lim, Y. M. Lam, M. Grätzel, S. Mhaisalkar and T. C. Sum, *Science*, 2013, **342**, 344–347.

7 S. D. Stranks, G. E. Eperon, G. Grancini, C. Menelaou, M. J. P. Alcocer, T. Leijtens, L. M. Herz, A. Petrozza and H. J. Snaith, *Science*, 2013, **342**, 341–344.

8 J. H. Noh, S. H. Im, J. H. Heo, T. N. Mandal and S. I. Seok, *Nano Lett.*, 2013, **13**, 1764–1769.

9 G. E. Eperon, V. M. Burlakov, P. Docampo, A. Goriely and H. J. Snaith, *Advanced Functional Materials*, 2014, **24**, 151–157.

10 Z. Tan and et al, *Nature Nanotech.*, 2014, 687–92.

11 F. Deschler and et al, *J. Phys. Chem. Lett.*, 2014, **5**, 1421–26.

12 M. Saliba and et al, *Adv. Mater.*, 2015.

13 S. D. Stranks and H. Snaith, *Nature Nanotech.*, 2015, **10**, 391–402.

14 A. Kojima, K. Teshima, Y. Shirai and T. Miyasaka, *Journal of the American Chemical Society*, 2009, **131**, 6050–6051.

15 B. V. Lotsch, *Angewandte Chemie International Edition*, 2014, **53**, 635–637.

16 H. J. Snaith, *The Journal of Physical Chemistry Letters*, 2013, **4**, 3623–3630.

17 J.-Y. Jeng, Y.-F. Chiang, M.-H. Lee, S.-R. Peng, T.-F. Guo, P. Chen and T.-C. Wen, *Advanced Materials*, 2013, **25**, 3727–3732.

18 D. Liu and T. L. Kelly, *Nature Photonics*, 2014, **8**, 133–138.

19 Q. Chen, H. Zhou, Z. Hong, S. Luo, H.-S. Duan, H.-H. Wang, Y. Liu, G. Li and Y. Yang, *Journal of the American Chemical Society*, 2014, **136**, 622–625.

20 P.-W. Liang, C.-Y. Liao, C.-C. Chueh, F. Zuo, S. T. Williams, X.-K. Xin, J. Lin and A. K.-Y. Jen, *Advanced Materials*, 2014, **26**, 3748–3754.

21 J. T.-W. Wang, J. M. Ball, E. M. Barea, A. Abate, J. A. Alexander-Webber, J. Huang, M. Saliba, I. Mora-Sero, J. Bisquert, H. J. Snaith and R. J. Nicholas, *Nano Letters*, 2014, **14**, 724–730.

22 V. D'Innocenzo, G. Grancini, M. J. P. Alcocer, A. R. S. Kandada, S. D. Stranks, M. M. Lee, G. Lanzani, H. J. Snaith and A. Petrozza, *Nature Communications*, 2014, **5**, year.

23 M. Hirasawa, T. Ishihara, T. Goto, K. Uchida and N. Miura, *Physica B: Condensed Matter*, 1994, **201**, 427 – 430.

24 E. Menéndez-Proupin, P. Palacios, P. Wahnón and J. C. Conesa, *Phys. Rev. B*, 2014, **90**, 045207.

25 J. Even, L. Pedesseau and C. Katan, *The Journal of Physical Chemistry C*, 2014, **118**, 11566–11572.

26 Y. Yamada, T. Nakamura, M. Endo, A. Wakamiya and Y. Kanemitsu, *Photovoltaics, IEEE Journal of*, 2015, **5**, 401–405.

27 Q. Lin, A. Armin, R. C. R. Nagiri, P. Burn and P. Meredith, *Nature Photonics*, 2015, **9**, 106–112.

28 A. Miyata, A. Mitioglu, P. Plochocka, O. Portugall, J. Tse-Wei Wang, S. D. Stranks, H. J. Snaith and R. J. Nicholas, *Nature Physics*, 2015, **11**, 582–U94.

29 W. Yang, J. H. Noh, N. Jeon, Y. Kim, S. Ryu, J. Seo and Seok;, *Science*, 2015, **348**, 1234–1237.

30 T. Umebayashi, K. Asai, T. Kondo and A. Nakao, *Phys. Rev. B*, 2003, **67**, 155405.

31 M. Kim, J. Im, A. J. Freeman, J. Ihm and H. Jin, *Proceedings of the National Academy of Sciences*, 2014, **111**, 6900–6904.

32 K. Watanabe, K. Ushida and N. Miura, *Phys. Rev. B*, 2003, **68**, 155312.

33 P. C. Makado and N. C. McGill, *Journal of Physics C: Solid State Physics*, 1986, **19**, 873.

34 P. Umari, E. Mosconi and F. De Angelis, *Scientific Reports*, 2014, **4**, 4467.

35 J. Even, L. Pedesseau, C. Katan, M. Kepenekian, J.-S. Lauret, D. Sapori and E. Delporte, *J. Phys. Chem. C*, 2015.

36 J. Even, L. Pedesseau, A. Dupertuis, M, J.-M. Jancu and C. Katan, *Phys. Rev. B*, 2012, **86**, 205301.

37 H.-H. Fang, R. Raissa, M. Abdu-Aguye, S. Adjokatse, G. Blake, J. Even and M. Loi, *Adv. Funct. Mater.*, 2015, **25**, 2378–2385.

38 C. Wehrenfennig, M. Liu, H. Snaith, M. Johnston and L. Herz, *Energ. Environ. Sci.*, 2014, **7**, 2269–2275.

39 F. Brivio, K. Butler, A. Walsh and M. van Schilfgaarde, *Phys.*

Rev. B, 2014, **89**, 155204.
40 J. Pollman and H. Büttner, *Solid State Communications*, 1975, **17**, 1171–1174.
41 E. Kane, *Phys. Rev. B*, 1978, **18**, 6849–6855.
42 E. E. Menéndez-Proupin, C. Beltrán Ríos and P. Wahnón, *physica status solidi (RRL)*, 2015, **9**, 559–563.
43 N. Onoda-Yamamuro, T. Matsuo and H. Suga, *J. Phys. Chem. Solids*, 1990, **51**, 1383–95.
44 H. Kunugita, T. Hashimoto, Y. Kiyota, Y. Udagawa, Y. Takeoka, Y. Nakamura, J. Sano, T. Matsushita, T. Kondo, T. Miyasaka and K. Ema, *Chem. Lett.*, 2015, **44**, 852–854.
45 G. Behnke, H. Buttner and J. Pollmann, *Solid State Communications*, 1978, **20**, 873–876.
46 A. Poglitsch and D. Weber, *J. Phys. Chem. Phys.*, 1987, **87**, 6373–6378.
47 A. M. Soufliani, F. Huang, P. Reece, R. Sheng, A. Ho-Ballie and M. A. Green, *Appl. Phys. Lett.*, 2015, **107**, 231902.
48 J. H. Heo, S. H. Im, J. H. Noh, T. N. Mandal, C.-S. Lim, J. A. Chang, Y. H. Lee, H.-j. Kim, A. Sarkar, M. K. Nazeeruddin, M. Graetzel and S. I. Seok, *Nature photonics*, 2013, **7**, 487–492.
49 R. J. Nicholas, P. Y. Solane and O. Portugall, *Phys. Rev. Lett.*, 2013, **111**, 096802.
50 O. Portugall, N. Puhlmann, H. U. Müller, M. Barczewski, I. Stolpe and M. von Ortenberg, *Journal of Physics D: Applied Physics*, 1999, **32**, 2354.

7 Table of Contents Entry

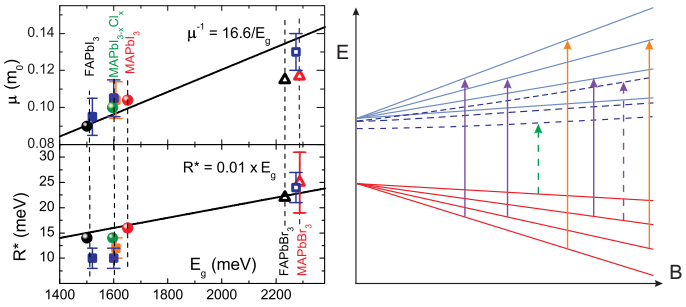

Fig. 7 The reduced effective mass (μ) and the excitonic Rydberg (R^*) are measured by magneto-optics for methylammonium and formamadinium perovskite semiconductors.